RSC Advances

PAPER

View Article Online
View Journal | View Issue

Cite this: *RSC Adv.*, 2026, **16**, 6768

Evaluation of novel multifunctional polymeric Schiff bases as anticorrosive agents for the medical grade 316L stainless steel

Aisha Hendy,[a] Jehan El-Nady,[b] Asmaa Nour,[c] Safaa M. Ali,[d] T. M. Tamer,[e] Amal S. I. Ahmed,[a] Rabab Mohamed Abou Shahba[a] and Nazly Hassan *[c]

In the field of biomaterials, the 316L stainless steel (316L SS) alloy is utilized in several countries as a temporary biomaterial without any prior treatment. In this work, corrosion protection and biocompatibility enhancements of the 316L SS alloy were performed. The influence of recently synthesized novel antibacterial, antimicrobial, and antioxidant polymeric materials, as corrosion inhibitors, on the 316L stainless steel surface was investigated. Initially, the primary amino groups of casein were reacted with the active carbonyl group of cinnamaldehyde to yield casein–cinnamadehyde (Ca–Cin) Schiff bases. These Schiff bases were then allowed to interact with the 316L SS alloy, resulting in self-assembled monolayers (SAMs) covering its surface. The features of these SAMs were then evaluated under simulated body fluid (SBF) conditions by electrochemical methods. Results confirmed the formation of SAMs from the studied Schiff bases, serving as mixed-type inhibitors on the 316L SS surface *via* a charge transfer mechanism. Moreover, these materials displayed both concentration- and immersion time-dependent corrosion inhibition efficiency, which exceeded 90% at 1000 ppm for Ca–Cin6 after 120 minutes of immersion in its solution. The corrosion inhibition efficiencies of these Schiff bases were optimized by investigating their dependence on the studied variables. The calculated thermodynamic parameters pointed out spontaneous adsorption of the Schiff base molecules on the metallic surface, obeying the Langmuir adsorption isotherm. These results reinforce that the materials under investigation exhibit promising features for refining the 316L stainless steel surface for implant applications.

Received 5th September 2025
Accepted 30th December 2025

DOI: 10.1039/d5ra06705g

rsc.li/rsc-advances

1. Introduction

Biomaterials are biocompatible materials, either natural or synthetic, that are implanted into the human body to repair or replace damaged or diseased parts.[1–3] The essential feature of biomaterials is their implantation in direct contact with the human body. From a medical perspective, these materials must exhibit qualities such as superior bioactivity, excellent biocompatibility, controlled degradability, biological non-toxicity and non-allergenicity, modulus of elasticity, good mechanical properties, and superior wear and corrosion resistance.[1,4,5] Generally, ceramics, polymers, or metallic materials are used as biomaterials.[5–7] Among these, metallic biomaterials (*e.g.*, stainless steels, Mg alloys, Cr–Co alloys, and Ti or Ti alloys) are popular because of their significant characteristics, such as excellent mechanical and chemical properties and ease of fabrication.[8–10]

The medical-grade low-carbon 316L stainless steel is extensively employed as a temporary implanted material in several countries owing to its easy availability, low cost, reasonable durability, good mechanical properties, acceptable biocompatibility, and high corrosion resistance.[1,4,11] However, over time, it corrodes in the aggressive environment of human body fluids, resulting in the release of some toxic ions that may act as carcinogens or allergens. This process boosts inflammatory reactions and ultimately contributes to implant failure.[4,5,12] In order to address this problem, refining of the stainless-steel surface is substantially required.

The self-assembled monolayers (SAMs) approach is an ordinary and promising technique for modifying the surface of the metallic

[a]*Chemistry Department, Faculty of Science (Girls), Al-Azhar University, Nasr City, Cairo, Egypt*

[b]*Electronic Materials Department, Advanced Technology and New Materials Research Institute (ATNMRI), City of Scientific Research and Technological Applications (SRTA-City), New Borg El-Arab City, P. O. Box: 21934, Alexandria, Egypt*

[c]*Composites and Nanostructured Materials Research Department, Advanced Technology and New Materials Research Institute (ATNMRI), City of Scientific Research and Technological Applications (SRTA-City), New Borg El-Arab City, P. O. Box: 21934, Alexandria, Egypt. E-mail: na_hassan12@yahoo.com; nhassan@srtacity.sci.eg*

[d]*Nucleic Acid Research Department, Genetic Engineering and Biotechnology Research Institute (GEBRI), City of Scientific Research and Technological Applications (SRTA-City), P. O. Box: 21934, New Borg El-Arab City, Alexandria, Egypt*

[e]*Polymer Materials Research Department, Advanced Technology and New Materials Research Institute (ATNMRI), City of Scientific Research and Technological Applications (SRTA-City), New Borg El-Arab City, P. O. Box: 21934, Alexandria, Egypt*

implants. This method produces a thin passive layer that acts as a barrier against corrosion of the metallic surfaces.[13–15] SAMs are nano-sized, well-organized films regulated by non-covalent interactions, which are formed by the physical and/or chemical adsorption of densely packed organic molecules on metallic surfaces.[13,15] SAMs exhibit micro-nanoscale features, physicochemical characteristics, and long-term stability, which make them suitable and promising for medical applications.[14,16–19]

Due to their strong affinity for metallic surfaces, organic molecules that include polar functional group(s), heteroatom(s), multiple bonds, and/or aromatic ring(s) in their molecular structure are able to adsorb spontaneously onto metallic surfaces, forming SAMs.[20–22] In this regard, Schiff bases have been previously considered as valuable materials to be utilized against metallic corrosion in aggressive environments.[17,23–27] The inhibition efficiency of Schiff bases is rationalized to the entity of a specific functional azomethine group (–RC═N–) and any electronegative heteroatoms in the molecular moiety.[17,23,26,28,29]

In this study, novel non-toxic antibacterial, antimicrobial, and antioxidant Schiff bases were synthesized in our laboratory[30] from the interaction of casein with cinnamaldehyde (a phenolic compound) with different degrees of substitution. These synthesized Schiff bases were suggested to create SAMs on the medical-grade 316L SS surface. Consequently, these Schiff bases were investigated as anticorrosive materials in SBF conditions using electrochemical tools. The effect of concentrations of the Schiff bases and different immersion time intervals was also studied. Analyzing and optimizing corrosion inhibition efficiency data was investigated through the response surface modeling (RSM) methodology by examining the impact of its reliance on the factors under study. Moreover, thermodynamic calculations were also performed.

2. Materials and methods

2.1. Materials

Casein bovine (Sigma, Germany) was dissolved in sodium hydrogen carbonate solution (99%, Fluka, Germany). Cinnamaldehyde (98%) was purchased from Scharlau, Spain. The components of the simulated body fluid (SBF), mentioned in ref. 31, are dissolved in double-distilled water. The SBF is freshly prepared according to ref. 32.

2.2. Methods

2.2.1. Synthesis of Schiff bases. The Schiff bases were synthesized by reacting casein's primary amino groups with cinnamaldehyde's active carbonyl group with different degrees of substitution (from Ca–Cin1 to Ca–Cin6), as presented in Fig. 1. More details can be found in ref. 30.

2.2.2. Preparation of metallic specimens. A sheet of 316L SS, with chemical composition presented in Table 1, was cut into small specimens with dimensions of 70 mm × 10 mm × 2 mm ($L \times W \times T$). More details are mentioned in ref. 31. Before each experiment, these specimens were polished to obtain a mirror-finish surface with different grades of emery paper (320, 400, 500, 600, and 1200). Only a 2 × 1 cm^2 area was selected for exposure to the electrolyte solution, whereas the rest of the specimen was covered with coat material and Teflon tape. After that, the metallic specimens were thoroughly rinsed with acetone to dislodge fine polishing debris and remove any contaminants or residual abrasive metallic particles that may interfere with the formation of SAMs. Then, the specimens were washed with double-distilled water and finally dried to be used for measurements.

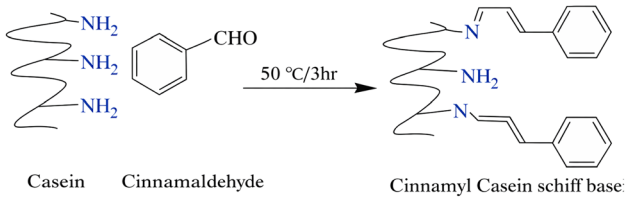

Fig. 1 Schematic of the synthesis of casein–cinnamaldehyde Schiff bases.[30]

2.2.3. Formation of self-assembled monolayers (SAMs). The 316L SS specimens were immersed in 0.1 M aqueous $NaHCO_3$ solution containing different concentrations (100, 300, 500, 700, and 1000 ppm) of casein–cinnamaldeyde Schiff bases to allow the formation of SAMs on the specimens' surface. The $NaHCO_3$ solution was selected because the casein Schiff bases are typically dissolved and activated in mild alkaline carbonate buffers.[30,33] Additionally, the $NaHCO_3$ solution is non-aggressive toward the 316L SS alloy. The mentioned Schiff bases were prepared by reacting cinnamaldehyde with casein at various degrees of substitution (Ca–Cin1, Ca–Cin2, Ca–Cin3, Ca–Cin4, Ca–Cin5, and Ca–Cin6).[30] The samples were then immersed at ambient temperature for 60, 90, and 120 minutes in the SAMs' solutions.

2.2.4. Electrochemical measurements. A three-electrode cell was used for the investigation. Blank and treated 316L SS samples were used as the working electrodes. A platinum wire and a saturated calomel electrode were employed as counter and reference electrodes, respectively. The experiments were performed at 37 ± 0.2 °C in 100 mL of freshly prepared simulated body fluid (SBF) electrolytic solution. All the experiments were performed in triplicate to ensure reproducibility and accuracy; subsequently, the optimal results were adopted for analysis.

2.2.4.1. Tafel polarization measurements. Before each experiment, to acquire the steady-state conditions, the electrodes were maintained in the electrolyte solution at open-circuit potential (OCP) for approximately 10 minutes. Such a short stabilization time is adequate, as the presence of SAMs enables fast potential stabilization. The measurements were performed at a scan rate (dE/dt) of 0.5 mV s^{-1} in the potential range $-250 > E_{SCE} > 250$ mV. A Voltalab potentiostat/galvanostat (PGZ 301 model, Radiometer Analytical, France) utilizing VoltaMaster software Version 4.0 was used. The inhibition efficiency ($\eta\%$) of the inhibitors and their surface coverage (θ) were calculated based on eqn (1) and (2):[34–37]

$$\eta\% = \frac{i^{\circ}_{corr} - i_{corr}}{i^{\circ}_{corr}} \times 100 \quad (1)$$

$$\theta = \frac{\eta\%}{100} \quad (2)$$

Table 1 Chemical composition of 316L stainless steel

Element	C	Mn	Si	S	P	Mo	Cr	Ni	Co	Cu	Al
Percentage	0.024	1.89	0.512	0.0092	0.0115	2.08	17.33	12.95	0.0712	0.178	0.0193

where i°_{corr} and i_{corr} are the corrosion current density of the blank and treated SS samples, respectively.

2.2.4.2. Electrochemical impedance study (EIS). The EIS was performed using a potentiostat (model AutoLab 87070) with an amplitude of 10 mV in the 0.1–10^5 Hz frequency range. The data were analyzed with a frequency response analyzer (FRA) impedance module using Nova 1.11 software and then illustrated as Nyquist and Bode plots. The data were interpreted depending on particular equivalent circuits. The inhibition efficiency was computed according to eqn (3):[25–27,38]

$$\eta\% = \frac{R_{ct} - R^{\circ}_{ct}}{R_{ct}} \times 100 \quad (3)$$

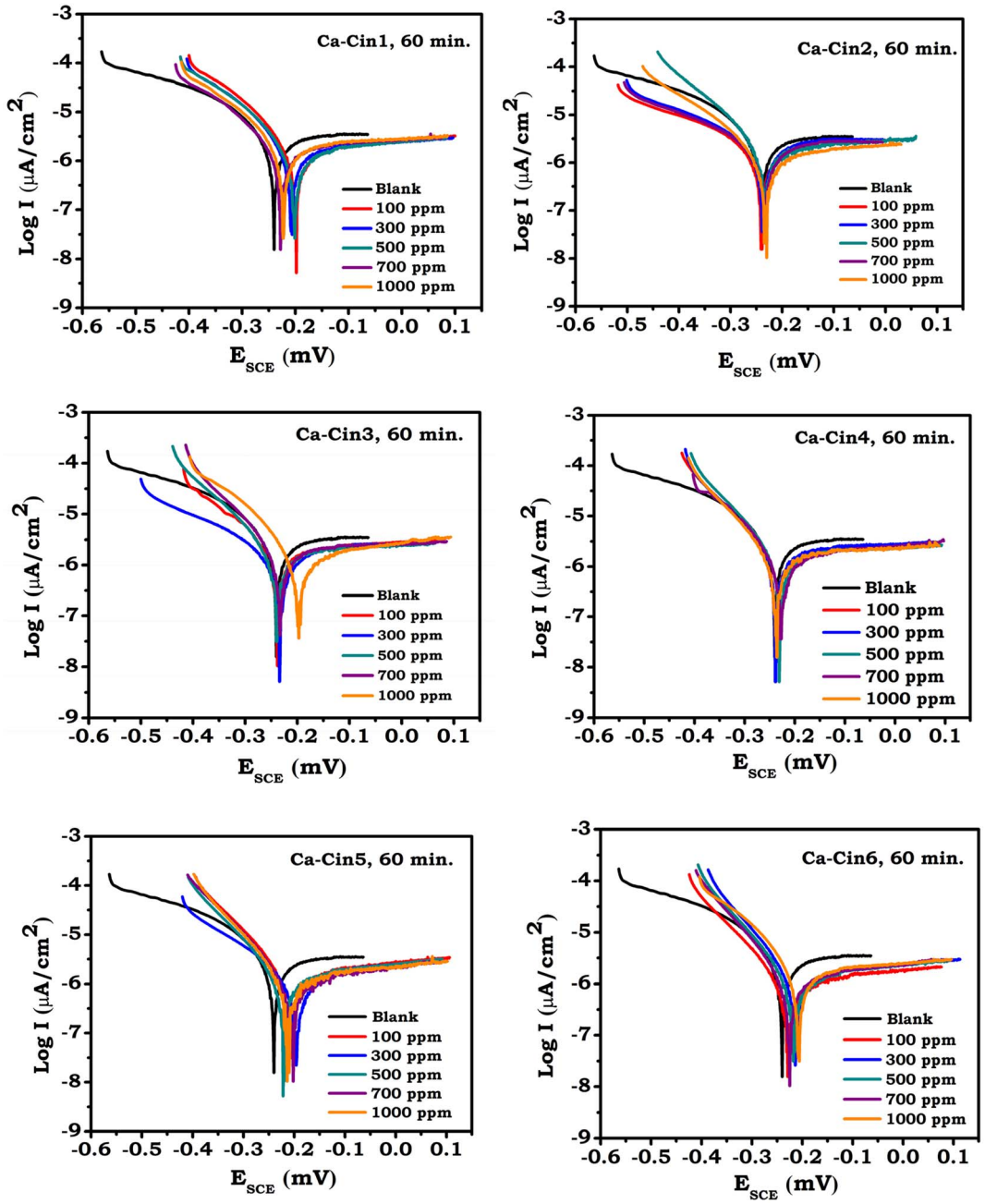

Fig. 2 Tafel curves at 37 ± 0.2 °C in SBF solutions of blank and immersed SS specimens for 60 min in Schiff base solutions of different concentrations. dE/dt = 0.5 mV s^{-1}.

where R_{ct}° and R_{ct} are the charge transfer resistance values of the blank and treated electrodes, respectively.

2.2.5. Treated sample appearance. Visual observation was considered to verify the accuracy of the electrochemical results and to ensure that the samples did not undergo corrosion in the Schiff base solution over time. A photograph was taken of a sample after two hours of immersion in the Schiff base solution, followed by electrochemical measurements conducted in the SBF solution.

2.2.6. Reliance of corrosion inhibition efficiency on the studied variables. The parameters affecting the corrosion process and its inhibition efficiency were analyzed and optimized. A correlation between the examined parameters, namely, the concentrations of Schiff base solutions and immersion times of the samples, and the inhibition performance was established. The optimization process and data analysis were clarified with Statistica, a statistical software.

3. Results and discussions

3.1. Electrochemical measurements

3.1.1. Tafel polarization technique. Fig. 2 displays the Tafel curves at 37 ± 0.2 °C in SBF of bare and immersed SS samples at various concentrations of the Schiff base solutions (from Ca–Cin1 to Ca–Cin6, respectively) at an immersion time of 60 minutes with a 0.5 mV s^{-1} scan rate in the $-250 > E_{SCE} > 250$ mV potential range.

As presented in Fig. 2, a slight positive shift is observed in the corrosion potential (E_{corr}) values of the modified samples relative to the blank one, suggesting the formation of SAMs by Schiff bases, pointing out their performance on the SS surface. The electrochemical parameters obtained from Tafel curves, besides the η% and θ values of the treated electrodes calculated from eqn (1) and (2), are listed in Table 2.

As illustrated in Table 2, the positive shift of E_{corr} is less than ±85 mV in the case of the treated electrodes. This indicates that the Schiff bases are classified as mixed-type inhibitors[16,21,24] with a slightly anodic predominance. This outcome is also supported by the shift of the cathodic and anodic slope values (β_c and β_a, respectively), which is greater for β_a,[17,39–42] as demonstrated in Table 2.

Moreover, lower corrosion current density (i_{corr}) values were obtained for the treated electrodes than for the blank one. Additionally, the effect of Schiff bases increases with increasing concentration of their solutions. This is because of the increase in the number of molecules approaching the metallic surface. Consequently, the rate of molecular interaction with the active

Table 2 Electrochemical parameters at 37 ± 0.2 °C in SBF solutions of blank and immersed SS specimens for 60 min in Schiff base solutions of different concentrations

Schiff bases	Conc. (ppm)	E_{corr} (mV)	i_{corr} (μA cm^{-2})	β_a (mV)	β_c (mV)	Corrosion rate (μm per year)	θ	η%
Blank	—	−242	3.232	121	−231	37.92	—	—
Ca–Cin1	100	−201	1.731	137	−138	20.30	0.4643	46.43
	300	−209	1.633	170	−141	19.16	0.4945	49.45
	500	−202	1.549	148	−144	18.16	0.5207	50.07
	700	−229	1.519	202	−153	17.81	0.5300	53.00
	1000	−224	1.496	227	−140	17.55	0.5369	53.69
Ca–Cin2	100	−241	1.276	332	−277	14.97	0.6049	60.49
	300	−240	1.239	491	−115	14.39	0.6166	61.66
	500	−234	1.227	467	−226	14.12	0.6203	62.03
	700	−236	1.128	394	−239	13.22	0.6509	65.09
	1000	−233	1.015	436	−150	11.89	0.6857	68.57
Ca–Cin3	100	−240	1.055	750	−137	12.37	0.6734	67.34
	300	−235	0.936	734	−236	10.97	0.7104	71.04
	500	−239	0.901	702	−109	10.56	0.7209	72.09
	700	−234	0.836	749	−100	10.16	0.7411	74.11
	1000	−199	0.741	407	−101	8.690	0.7707	77.07
Ca–Cin4	100	−239	0.7848	648	−99	9.201	0.7571	75.71
	300	−240	0.7661	633	−98	8.985	0.7629	76.29
	500	−231	0.7349	553	−94	8.619	0.7726	77.26
	700	−229	0.7249	529	−107	8.591	0.7757	77.57
	1000	−238	0.6439	620	−94	7.551	0.8007	80.07
Ca–Cin5	100	−208	0.6691	761	−96	7.845	0.7929	79.29
	300	−197	0.6604	808	−159	7.744	0.7956	79.56
	500	−222	0.5930	776	−94	6.954	0.8165	81.65
	700	−206	0.5805	746	−97	6.801	0.8203	82.03
	1000	−215	0.5376	779	−89	6.304	0.8336	83.36
Ca–Cin6	100	−234	0.6129	339	−67	7.187	0.8103	81.03
	300	−214	0.5732	329	−87	6.721	0.8226	82.26
	500	−219	0.5547	373	−91	6.504	0.8283	82.83
	700	−227	0.5441	370	−90	6.354	0.8316	83.16
	1000	−218	0.4735	344	−84	5.559	0.8535	85.35

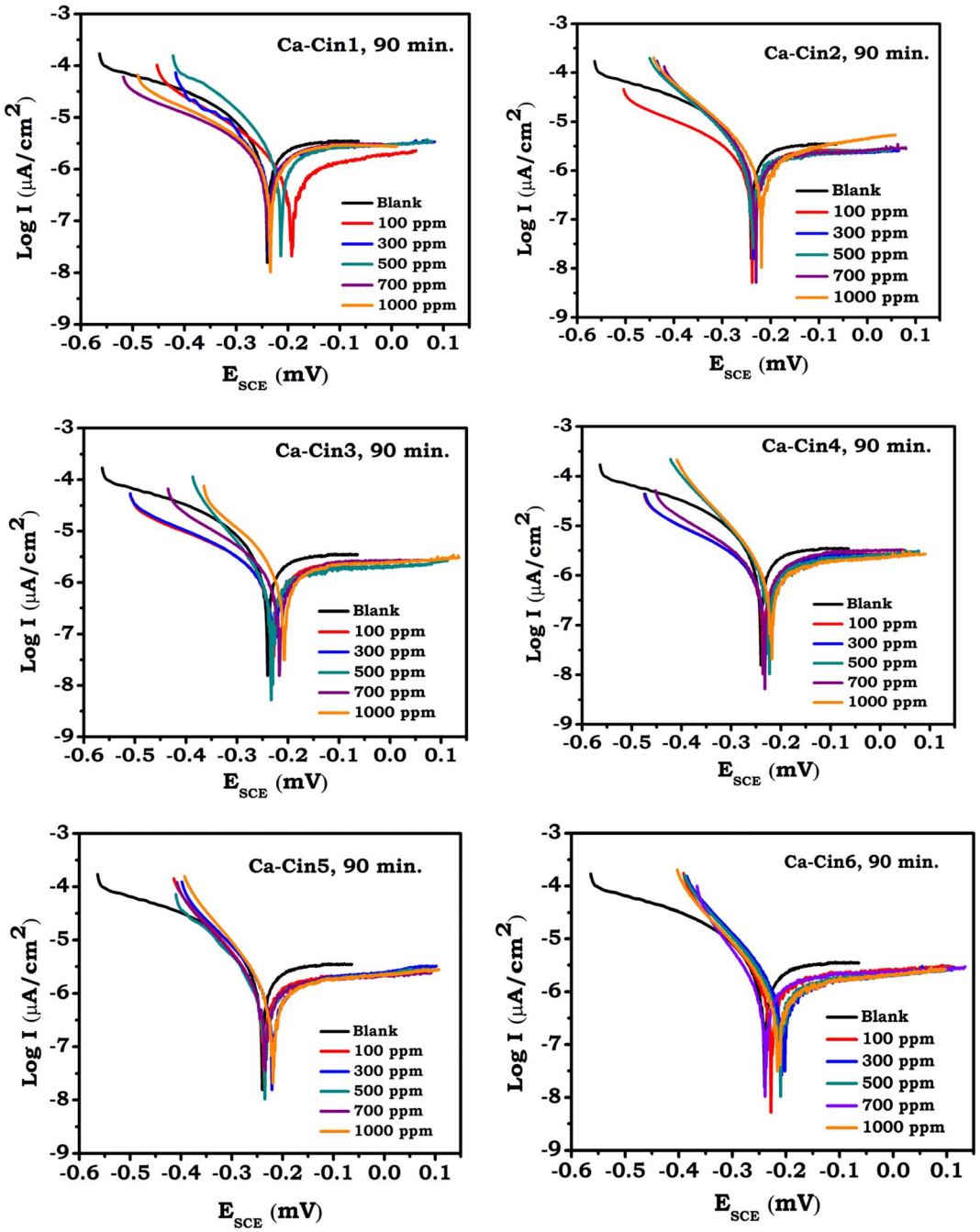

Fig. 3 Tafel curves at 37 ± 0.2 °C in SBF solutions of blank and immersed SS specimens for 90 min in Schiff base solutions of different concentrations. $dE/dt = 0.5$ mV s^{-1}.

sites of the metal surface will increase, leading to greater adsorption.[43,44]

The maximum corrosion inhibition efficiency (~53.7, 68.6, 77.7, 80, 83.4, and 85.4%) was obtained at 1000 ppm for Ca–Cin1, Ca–Cin2, Ca–Cin3, Ca–Cin4, Ca–Cin5, and Ca–Cin6, respectively. These maximum values illustrate an increase in corrosion inhibition efficiency is achieved, rising from 54% to 85%. This performance is attributed to the increase in the degree of substitution of the amino group present in the casein with cinnamaldehyde molecules and the C=N bond formation increases the number of carbonyl and phenolic groups. These results indicate the formation of SAMs and demonstrate their corrosion inhibition efficiency.[16,21,22]

To examine the impact of immersion time on SAMs formation, the 316L SS corrosion behavior was tested after 90 min of immersion in polymeric solutions. The acquired polarization curves are illustrated in Fig. 3. A similar behavior, as in the case of 60 minutes of immersion, was observed. However, a further corrosion rate reduction and enhanced corrosion inhibition efficiency were achieved (from ~61% to 86%) in the same sequence, as demonstrated in Table 3. These findings may be attributed to the densely packed, more compact SAMs on the

Table 3 Electrochemical parameters at 37 ± 0.2 °C in SBF solutions of blank and immersed SS specimens for 90 min in Schiff base solutions of different concentrations

Schiff bases	Conc. (ppm)	E_{corr} (mV)	i_{corr} (μA cm^{-2})	β_a (mV)	β_c (mV)	Corrosion rate (μm per year)	θ	η%
Blank	—	−242	3.232	121	−231	37.92	—	—
Ca–Cin1	100	−195	1.461	539	−156	17.13	0.5479	54.79
	300	−238	1.409	358	−168	16.35	0.5638	56.38
	500	−224	1.351	361	−136	15.84	0.5818	58.18
	700	−239	1.303	477	−244	15.28	0.5967	59.67
	1000	−235	1.264	583	−212	14.83	0.6087	60.87
Ca–Cin2	100	−239	1.137	345	−242	13.34	0.6479	64.79
	300	−237	1.092	528	−116	12.81	0.6618	66.18
	500	−238	1.079	578	−118	12.66	0.6659	66.59
	700	−232	1.007	500	−112	11.81	0.6882	68.82
	1000	−220	0.994	554	−121	11.66	0.6922	69.22
Ca–Cin3	100	−231	0.920	464	−239	10.79	0.7152	71.52
	300	−230	0.901	449	−200	10.57	0.7210	72.10
	500	−233	0.862	413	−81	10.11	0.7331	73.31
	700	−218	0.827	353	−165	9.701	0.7440	74.40
	1000	−209	0.820	542	−110	9.621	0.7461	74.61
Ca–Cin4	100	−236	0.7591	398	−202	8.902	0.7651	76.51
	300	−234	0.7366	366	−204	8.638	0.7720	77.20
	500	−226	0.7194	402	−95	8.436	0.7774	77.74
	700	−235	0.7131	402	−165	8.362	0.7793	77.93
	1000	−221	0.6282	443	−98	7.363	0.8056	80.56
Ca–Cin5	100	−238	0.6472	468	−94	7.589	0.7997	79.97
	300	−221	0.6164	402	−100	7.060	0.8092	80.92
	500	−236	0.5881	491	−104	6.947	0.8180	81.80
	700	−235	0.5651	465	−94	6.627	0.8251	82.51
	1000	−220	0.5193	440	−85	6.081	0.8393	83.93
Ca–Cin6	100	−228	0.5869	285	−86	6.884	0.8184	81.84
	300	−207	0.5522	350	−89	6.493	0.8291	82.91
	500	−213	0.5346	365	−87	6.269	0.8345	83.45
	700	−240	0.5154	302	−94	6.045	0.8405	84.05
	1000	−216	0.4774	393	−90	5.598	0.8522	85.22

316L SS surface, which required more time,[16,22] exhibiting a higher effect in reducing the corrosion rate. The obtained electrochemical parameters are also presented in Table 3.

Furthermore, the corrosion behavior of the 316L SS samples immersed for 120 minutes in the polymeric solutions is demonstrated in the Tafel curves (Fig. 4). The electrochemical parameters and the calculated values of θ and η% are collected in Table 4.

The data illustrated in Tables 2–4 indicate that the corrosion rates decrease not only with increasing the concentration of different Schiff bases but also with longer immersion times in Schiff base solutions. However, the corrosion inhibition efficiencies increase, following the same trend, and the Schiff base (Ca–Cin6) always records the highest inhibition efficiency. These consequences may be interpreted as the creation of more ordered, compact, dense-packed SAMs, which require longer immersion times to achieve.[16,22,45,46]

For a clear comparison between the influence of the six Schiff bases on the corrosion process of 316L SS in SBF, Fig. 5 displays their corrosion inhibition efficiencies at different immersion times and optimum concentration (1000 ppm). As demonstrated in the figure, the corrosion inhibition efficiencies of all Schiff bases are increased, to some extent, with increasing immersion time in the SAMs' solutions. The inhibition efficiency order is clarified as Ca–Cin1 < Ca–Cin2 < Ca–Cin3 < Ca–Cin4 < Ca–Cin5 < Ca–Cin6. This may be attributed to the enhanced surface roughness resulting from the increased substitution of cinnamyl moieties, which leads to an increased specific surface area,[30] thereby facilitating the interaction with the 316L SS surface.

The corrosion inhibition efficiency of Schiff bases depends on the number of heteroatoms and C=N groups present in their molecules. As a result, the first polymeric Schiff base (Ca–Cin1) has the lowest corrosion inhibition efficiency since it contains fewer heteroatoms and polar functional groups than the other Schiff bases.[44,48] Alternatively, the Schiff base Ca–Cin6 exhibits superior corrosion inhibition performance as a result of multiple C=N bonds and polar functional groups in its moiety. This modification enhanced the electron-donating properties, leading to improved antioxidant potential *via* providing additional active sites in the organic molecules[30] to cover and protect the metallic surface. All these results suggested the formation of SAMs by Schiff bases on the 316L stainless steel surface, minimizing its corrosion rate.

3.1.2. Electrochemical impedance spectroscopy (EIS). As further evidence for the formation of SAMs, the electrochemical behavior of Schiff bases was examined using EIS and is presented as Nyquist and Bode plots. Fig. 6 shows the Nyquist plots in the SBF of bare and treated SS samples with different Schiff base solutions after 60 minutes of immersion. As is clear from

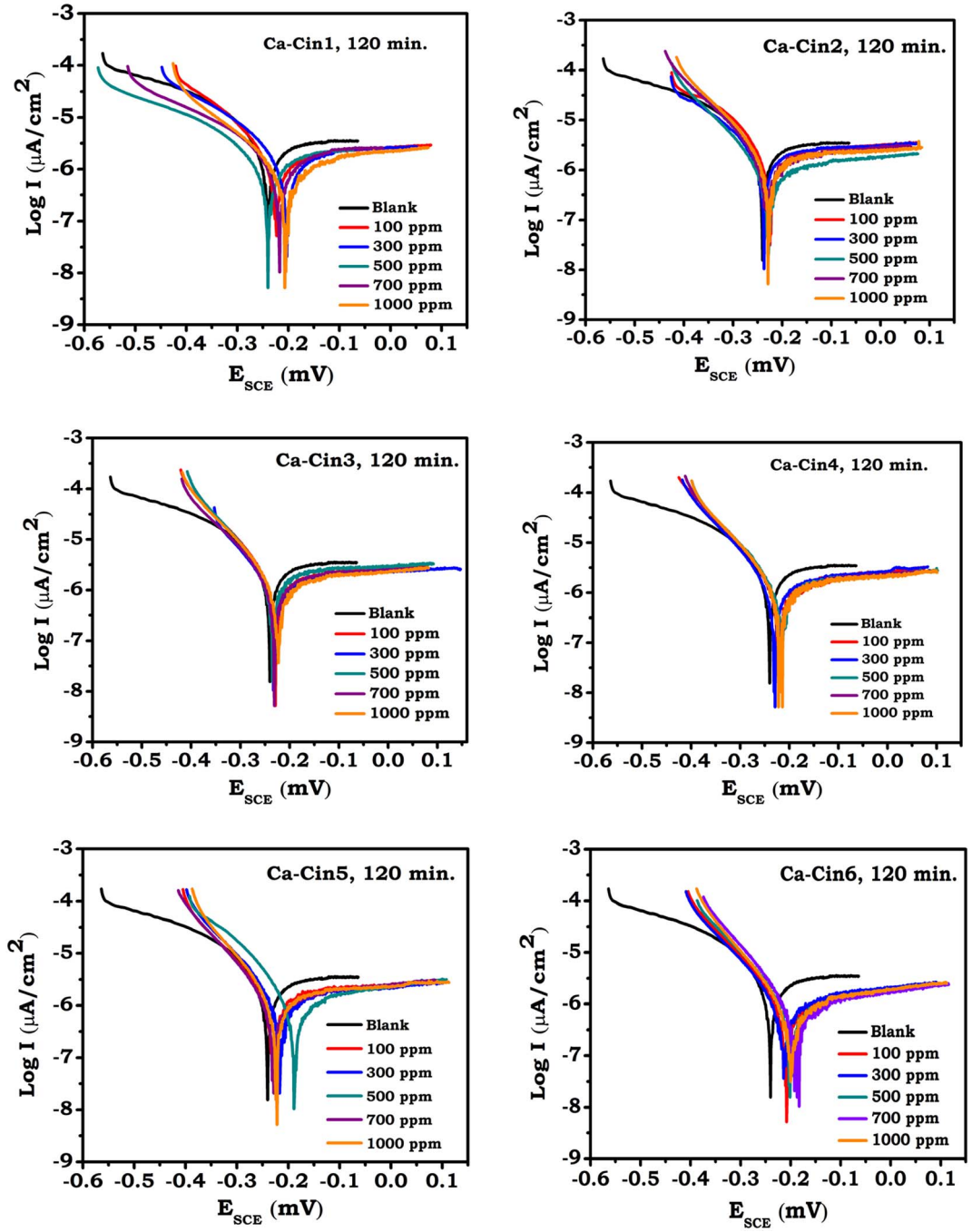

Fig. 4 Tafel curves at 37 ± 0.2 °C in SBF solutions of blank and immersed SS specimens for 120 min in Schiff base solutions of different concentrations. $dE/dt = 0.5$ mV s^{-1}.

Fig. 6, and as a result of surface roughness and inhomogeneity, a depressed incomplete semicircle is attained in the chosen frequency range for the blank and treated electrodes, indicating a charge transfer-controlled reaction.[27,48,49] This is further reinforced by single maxima acquired in the forthcoming Bode plots.[50–52] Moreover, the diameter of the semicircles increased for the treated electrodes with different Schiff base solutions, referring to the formation of SAMs.

A further increase in the diameter is achieved by increasing the concentration of polymeric cinnamyl casein Schiff base solutions and as a result of introducing more phenolic aldehyde groups of cinnamaldehyde in the casein's moiety,[30] which exhibit strong electron-donating properties, facilitating the charge transfer mechanism.

To fit the electrochemical data, equivalent circuits were proposed for the Nyquist plots of blank and treated electrodes ($\{R(Q[RW])\}$ and $\{R(RQ)\}$, respectively), as displayed in Fig. 7. The equivalent circuits comprise one electrical capacitance characterizing the double-layer capacitance, which is replaced by a constant phase element (CPE) owing to the non-homogeneity

Table 4 Electrochemical parameters at 37 ± 0.2 °C in SBF solutions of blank and immersed SS specimens for 120 min in Schiff base solutions of different concentrations

Schiff bases	Conc. (ppm)	E_{corr} (mV)	i_{corr} (μA cm^{-2})	β_a (mV)	β_c (mV)	Corrosion rate (μm per year)	θ	η%
Blank	0	−242	3.232	121	−231	37.92	—	—
Ca–Cin1	100	−225	1.310	250	−143	15.37	0.5945	59.45
	300	−204	1.222	251	−176	14.33	0.6218	62.18
	500	−241	1.105	262	−228	12.96	0.6578	65.78
	700	−219	1.062	268	−210	12.46	0.6712	67.12
	1000	−207	1.024	347	−136	12.10	0.6831	68.31
Ca–Cin2	100	−225	1.154	661	−178	13.45	0.6428	64.28
	300	−239	1.037	669	−133	12.16	0.6790	67.90
	500	−230	0.952	502	−101	11.17	0.7052	70.52
	700	−233	0.892	490	−106	10.46	0.7238	72.38
	1000	−229	0.863	633	−102	10.12	0.7328	73.28
Ca–Cin3	100	−231	0.862	380	−99	10.74	0.7331	73.31
	300	−234	0.821	515	−79	9.630	0.7459	74.59
	500	−236	0.792	473	−90	9.293	0.7548	75.48
	700	−232	0.754	419	−104	8.849	0.7665	76.65
	1000	−224	0.681	748	−97	7.990	0.7890	78.90
Ca–Cin4	100	−221	0.6888	441	−97	8.077	0.7868	78.68
	300	−231	0.6722	436	−95	7.883	0.7920	79.20
	500	−216	0.6455	416	−93	7.879	0.8002	80.02
	700	−224	0.6058	439	−95	7.570	0.8125	81.25
	1000	−220	0.5924	488	−93	7.194	0.8167	81.67
Ca–Cin5	100	−229	0.6234	560	−95	7.290	0.8071	80.71
	300	−217	0.6133	481	−96	7.251	0.8102	81.02
	500	−189	0.5757	586	−97	6.728	0.8218	82.18
	700	−230	0.5600	448	−91	6.567	0.8267	82.67
	1000	−224	0.5492	410	−84	6.335	0.8300	83.00
Ca–Cin6	100	−210	0.4908	833	−97	5.761	0.8481	84.81
	300	−214	0.4843	732	−99	5.679	0.8501	85.01
	500	−200	0.4712	702	−97	5.525	0.8542	85.42
	700	−192	0.3919	588	−88	4.595	0.8787	87.87
	1000	−201	0.3526	560	−86	4.182	0.8909	89.09

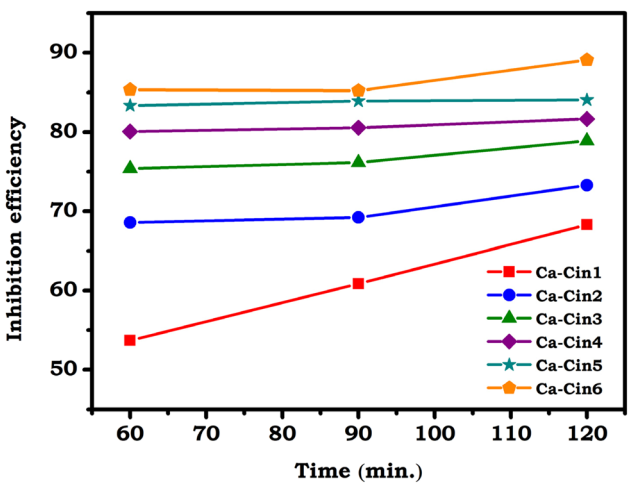

Fig. 5 Corrosion inhibition efficiency-immersion time curves derived from Tafel plots in SBF solutions of 316L SS samples immersed in solutions containning 1000 ppm of different Schiff base for various time intervals.

of the surface. The equivalent circuits also include R_s and R_{ct} representing solution resistance and charge transfer resistance, respectively. A Warburg element (W) is present only in the case of the bare electrode, indicating the diffusion process. The fitted data and the inhibition efficiency (η%) values, calculated based on eqn (3), are presented in Table 5.

As demonstrated in Table 5, the charge transfer resistance values (R_{ct}) in the case of immersed electrodes for 60 minutes are higher than in the case of the blank one. Moreover, there is a further increase in the R_{ct} values with increasing Schiff base concentration. The maximum inhibition efficiency (η%) values, which ranged from 83.41 to 87.24%, were obtained at 1000 ppm, indicating the formation of SAMs and their corrosion inhibition performance.

The influence of the immersion time of the 316L SS electrode in different polymeric solutions was also investigated by EIS. Figs. 1S and 2S demonstrate the Nyquist plots after 90 and 120 minutes of immersion, respectively, and the electrochemical parameters are collected in Tables 1S and 2S, respectively, as demonstrated in the supplementary information.

Comparing the data in Tables 5, 1S, and 2S reveals the increase in charge transfer resistance as the immersion time increases. The maximum inhibition performance values (ranging from 84.16 to 91.84%) were obtained after 120 minutes of immersion in the Schiff base solutions, as clarified in Table 2S. This may be attributed to the creation of SAMs on the SS surface, acting as a passive layer against the corrosive medium, which

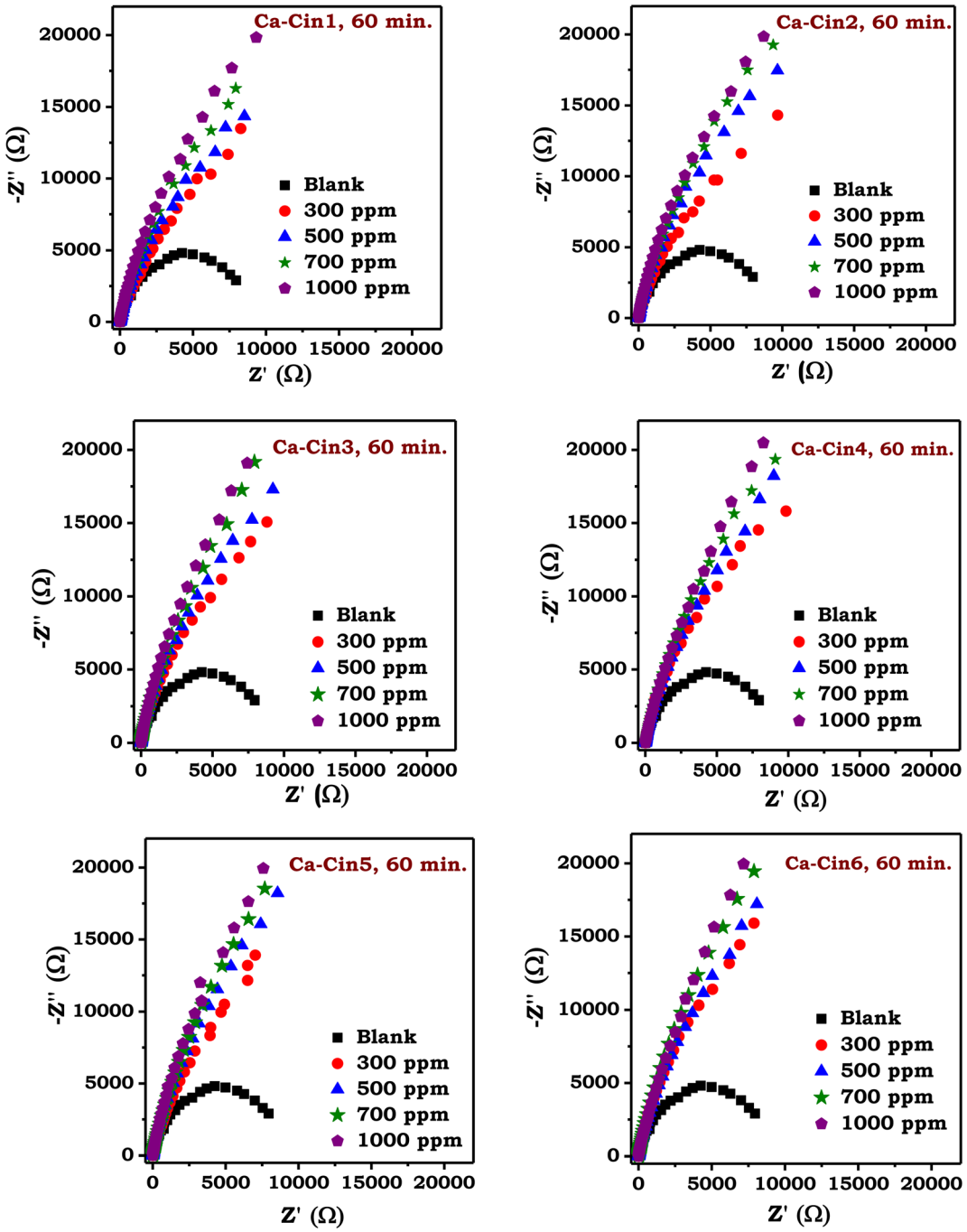

Fig. 6 Nyquist plots in the SBF solutions of blank and immersed SS specimens for 60 min in Schiff base solutions of different concentrations.

required longer immersion times for further rearrangement, regulation, and stabilization.[21,22,46,53] Ultimately, the results obtained from the electrochemical impedance studies are in good agreement with those of the Tafel polarization measurements. Additionally, it is worth noting that these Schiff bases displayed extremely high inhibition performance compared to absolute casein, which achieved only 50% under the same conditions.[54]

The electrochemical behavior of different Schiff bases was also demonstrated by Bode plots. However, there is no considerable change with different concentrations. Thus, only the Bode plots for the immersed electrodes in 1000 ppm solutions at different immersion time intervals (from 60 to 120 minutes) were selected to be presented. As displayed in Fig. 8, the data for the bare and treated electrodes exhibit only one time constant. These results are consistent with the semicircles achieved from Nyquist plots.[55–57]

Besides, for the treated electrodes, as the immersion time in the Schiff base solutions increases, the impedance modulus observed at lower frequencies increases to some extent, as illustrated in Fig. 8. Additionally, the phase angle exhibits a similar increase with the same trend and shifts to a lower frequency value, indicating the formation of SAMs on the SS surface and suggesting their inhibition behavior.[57–59]

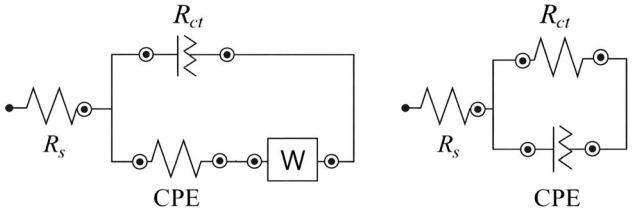

Fig. 7 Fitted equivalent circuits of the EIS data of the bare (left) and immersed (right) 316L SS samples in different Schiff base solutions (from Ca–Cin1 to Ca–Cin6) for 60 minutes.

3.2. Visual observation

To reinforce the previous findings and demonstrate that the sample did not exhibit any apparent corrosion as a result of immersion in the inhibitor solution, a photograph was taken of the sample showing its appearance after two hours of immersion in the inhibitor solution, followed by electrochemical measurements. In Fig. 9, area A represents the sample after polishing, immersion, and measurements, while area B illustrates the sample without any treatment. As is evident, there is no apparent change in the treated sample, and no signs of surface corrosion are present.

3.3. Reliance of corrosion inhibition efficiency on the studied variables

The inhibitory efficiency of various Schiff bases on 316L SS corrosion in SBF was analyzed and optimized. The two optimization factors employed were the inhibitor concentration (in ppm) and the immersion time (in min) of the 316L SS samples. Fig. 10 displays the correlation between the expected and experimental values.

The 3D surface plots, as shown in Fig. 10, illustrate the optimal conditions and the interaction between the investigated variables. Therefore, it is possible to estimate the ideal conditions for the Schiff base inhibition process of 316L SS corrosion in SBF solution. The data analysis revealed that when the inhibitor concentration increases, the inhibition efficiency increases. The same trend was obtained with longer immersion times.

These findings, which are consistent with Tafel polarization and impedance measurements, confirmed that the inhibitor molecules are initially adsorbed on the metal surface. Then, more time is required for the time-dependent rearrangement and regulation of organic molecules on the 316L SS surface, resulting in higher surface coverage and the formation of well-organized, stabilized, and compact SAMs, which subsequently improve the corrosion inhibition performance.[37,38,45,46] Finally, Ca–Cin6 was found to exhibit the highest inhibitory efficiency at 1000 ppm and 120 minutes of immersion.

3.4. Adsorption isotherm

The corrosion inhibition action of organic molecules on metallic surfaces depends on their nature of interaction with the metal surface and the extent of adsorption. This can be understood from adsorption isotherms, which give information

Table 5 Fitted EIS parameters at 37 ± 0.2 °C in SBF solutions of blank and immersed SS specimens for 60 min in Schiff base solutions of different concentrations

			CPE				
Schiff bases	Conc. (ppm)	R_s (Ω)	Y_{dl} (μMho)	n	R_{ct} (kΩ)	W (μMho)	η%
Blank	0	7.54	82.7	0.890	11.5	92.1	—
Ca–Cin1	300	9.97	83.4	0.861	35.0	—	67.14
	500	9.22	81.0	0.882	43.1		73.32
	700	10.9	76.8	0.902	51.5		77.67
	1000	10.8	66.1	0.903	69.3		83.41
Ca–Cin2	300	11.8	79.1	0.880	37.9	—	69.66
	500	10.4	71.1	0.908	49.9		76.95
	700	10.6	69.7	0.912	62.0		81.45
	1000	9.72	66.7	0.911	72.3		84.09
Ca–Cin3	300	10.6	74.8	0.899	40.3	—	71.46
	500	8.87	73.1	0.909	50.7		77.32
	700	9.05	72.4	0.912	66.4		82.68
	1000	12.9	72.1	0.909	79.4		85.52
Ca–Cin4	300	9.13	73.8	0.910	42.1	—	72.68
	500	11.8	70.3	0.901	54.3		78.82
	700	10.9	69.2	0.905	70.3		83.64
	1000	16.2	64.7	0.886	85.3		86.52
Ca–Cin5	300	15.1	81.3	0.862	49.8	—	76.91
	500	9.68	72.2	0.908	62.3		81.54
	700	10.8	73.0	0.890	79.9		85.61
	1000	13.2	69.9	0.897	88.3		86.98
Ca–Cin6	300	9.64	81.6	0.907	50.0	—	77
	500	11.5	76.3	0.895	60.1		80.87
	700	13.9	69.6	0.904	88.0		86.93
	1000	9.77	70.3	0.887	90.1		87.24

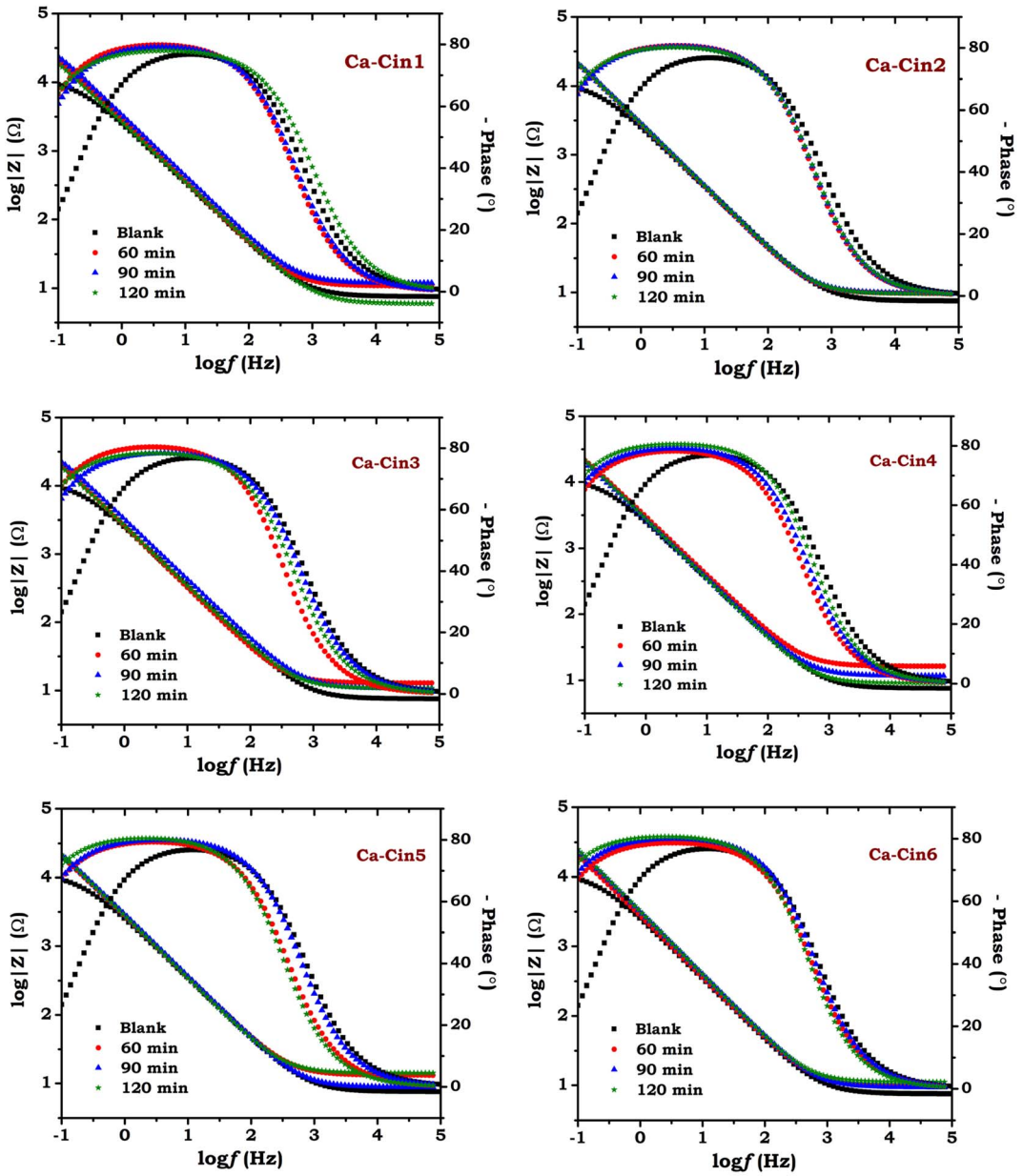

Fig. 8 Bode plots in SBF solutions of blank and immersed 316L SS specimens with various immersion times in 1000 ppm of Schiff base solutions.

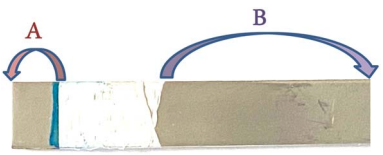

Fig. 9 Features of the 316L SS sample after two hours of immersion in the inhibitor solution, followed by electrochemical measurements (area A) and without any treatment (area B).

about the inhibitors' behavior and their interactions with the electrode surface.[24,27,43] Multiple adsorption isotherms are considered in thermodynamics. Depending on the obtained correlation coefficient values, very close to one, the data were fitted with the Langmuir isotherm,[24,36,57] as the surface coverage (θ) is related to the concentration of the adsorbed compound (C) as follows:[22,27,36]

$$\frac{C}{\theta} = \frac{1}{K_{ads}} + C \quad (4)$$

where K_{ads} is the adsorption equilibrium constant. A linear relationship is obtained from the plot of C/θ *versus* C, as shown in Fig. 11. This confirms that the adsorption process obeys the Langmuir adsorption isotherm. The values of K_{ads} obtained from the plots as the reciprocal of the intercept, the correlation coefficient (R^2), and the slope derived from Langmuir adsorption isotherms are presented in Table 6.

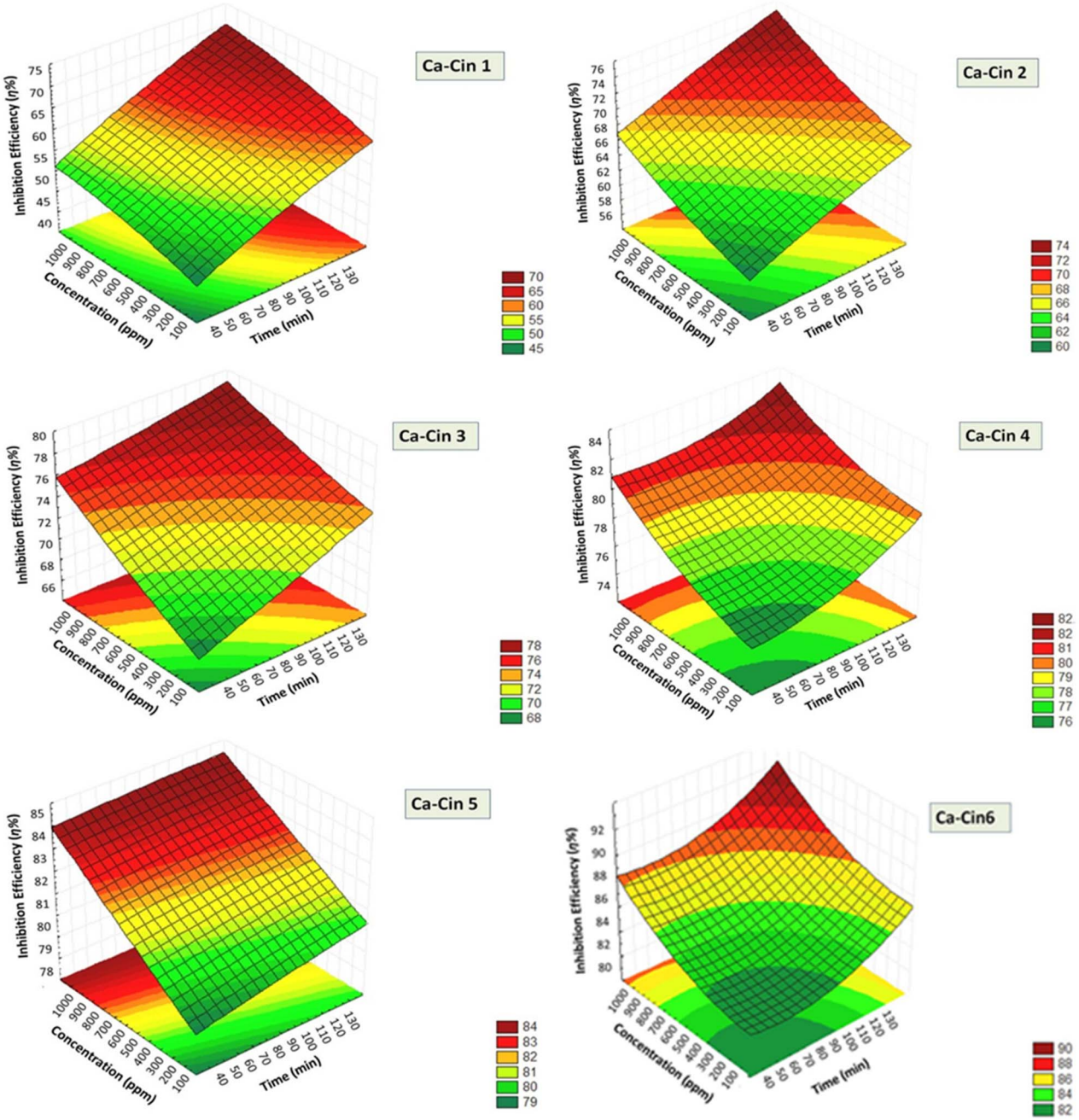

Fig. 10 Three-dimensional relationship demonstrating the corrosion inhibition efficiency (η%) dependence on the concentration of Schiff bases (in ppm) and immersion time (in min).

According to the determined K_{ads} values, the change in free energy of adsorption (ΔG°_{ads}) is computed based on eqn (5) and tabulated in Table 6:[43,55,60]

$$\Delta G^{\circ}_{ads} = -RT \ln(C_{sol} K_{ads}) \quad (5)$$

where T is the absolute temperature, R is the universal gas constant (equal to 8.315 J mol^{-1} K^{-1}), and C_{sol} is the molar concentration of solvent, which equals 55.5 mol dm^{-3} as the solvent is water.[35,57,59]

$$\Delta G^{\circ}_{ads} = -RT \ln(55.5 K_{ads}) \quad (6)$$

Thermodynamically, it is recognized that when ΔG°_{ads} has a negative sign, the adsorption process is spontaneous.[22,27,59] Generally, when the values of ΔG°_{ads} approach -20 kJ mol^{-1} or lower, a physisorption is expected because it is associated with electrostatic interactions of the electrode surface and charged inhibitor molecules.[22,24,59]

Moreover, when ΔG°_{ads} values are equal to or greater than -40 kJ mol^{-1}, it refers to chemisorption, which is associated with sharing or transferring electrons between inhibitor molecules and the SS surface by means of coordinated bonds.[16,24,61]

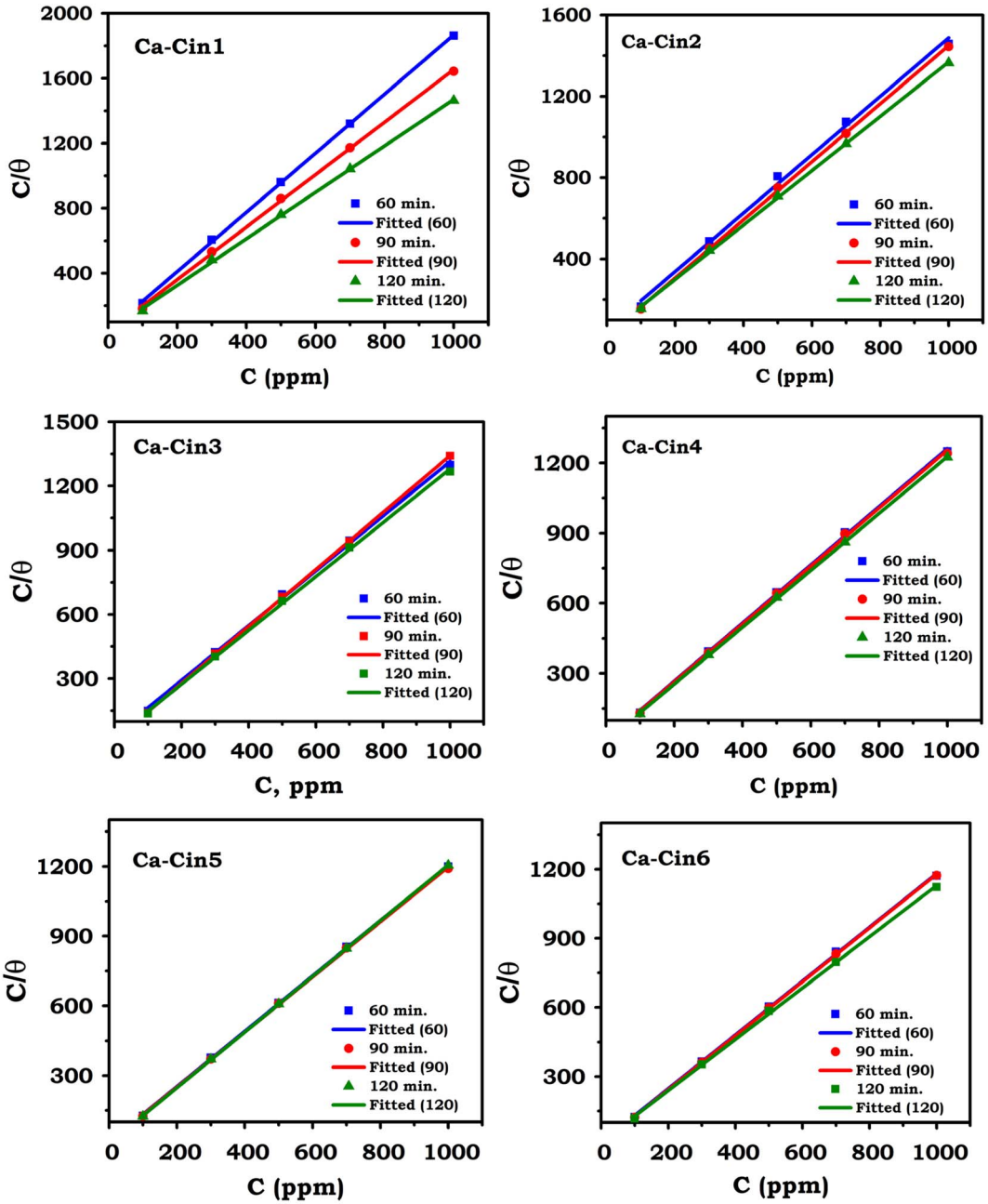

Fig. 11 Langmuir adsorption isotherm of the treated 316L SS samples with different Schiff bases at different immersion times.

In this study, ΔG°_{ads} values ranged from −30 to −39 kJ mol^{-1}. This indicates that the adsorption of Schiff bases on the stainless steel surface may be comprehensive, involving both physical and chemical adsorption.[27,35,42,62]

3.5. Proposed adsorption mechanism

The adsorption of the Schiff base SAMs on the metallic surface can proceed through one or more of the following interactions, either individually or in combination: (a) an electron donor–acceptor interaction between the vacant d-orbital of Fe atoms and imine (C=N) groups of the Schiff base molecules, which results in chemisorption,[16,44,63] (b) an electrostatic interaction between the heteroatoms of the Schiff base molecules and the metal surface (physisorption),[22,24,44,47,59] (c) interaction between the π-electrons of Schiff base molecules and the metal surface,[24,43,57,63] (d) due to the presence of amino groups, a release of one of their hydrogen atoms is probable, resulting in covalent bonding with the metal surface (chemisorption), and (e) chelation is also suggested between two heteroatoms in the Schiff base moiety and the metal surface to form five-membered rings.[16,24,64–69] Accordingly, a strong protective film is proposed to be formed on the SS surface predominantly due to chemisorption. The probabilities of both physical and chemical adsorption are demonstrated in Fig. 12.

Table 6 Adsorption parameters of the six Schiff bases on the 316L SS surface at different immersion times

		R^2			Slope			K_{ads} (M^{-1})			ΔG°_{ads} (kJ mol^{-1})		
Schiff base	Conc. (ppm)	60 min	90 min	120 min	60 min	90 min	120 min	60 min	90 min	120 min	60 min	90 min	120 min
Ca–Cin1	100	0.9996	0.9992	0.9993	1.22	1.21	1.23	8667	12 119	14 660	−33.71	−34.58	−35.07
	300							3260	4308	5480	−31.19	−31.91	−32.53
	500							2172	2782	3844	−30.15	−30.78	−31.62
	700							1610	2113	2916	−29.38	−30.08	−30.90
	1000							1159	1555	2155	−28.53	−29.29	−33.71
Ca–Cin2	100	0.9954	0.9994	0.9995	1.13	1.12	1.13	15 310	18 401	17 995	−35.18	−35.65	−35.95
	300							5360	6522	7050	−32.47	−32.97	−33.18
	500							3267	3986	4784	−31.2	−31.71	−32.18
	700							2663	3153	3743	−30.67	−31.11	−31.55
	1000							2181	2248	2742	−30.16	−30.23	−30.75
Ca–Cin3	100	0.9982	0.9998	0.9990	1.27	1.32	1.25	20 618	25 112	27 467	−35.94	−36.45	−36.68
	300							8176	8614	9784	−33.56	−33.70	−34.02
	500							5165	5493	6156	−32.38	−32.54	−32.83
	700							4089	4151	4689	−31.78	−31.81	−32.13
	1000							3361	2938	3739	−31.27	−30.92	−31.55
Ca–Cin4	100	0.9990	0.9990	0.9998	1.24	1.23	1.21	31 169	32 571	36 904	−37.01	−37.12	−37.45
	300							10 725	11 286	12 692	−34.26	−34.39	−34.69
	500							6795	6984	8010	−33.08	−33.16	−33.51
	700							4940	5044	6190	−32.26	−32.32	−32.84
	1000							4017	4144	4455	−31.73	−31.81	−32.00
Ca–Cin5	100	0.9997	0.9997	0.9999	1.19	1.18	1.15	38 285	39 925	41 840	−37.54	−37.65	−37.77
	300							12 974	14 136	14 229	−34.75	−34.97	−34.99
	500							8899	8989	9223	−33.78	−33.81	−33.87
	700							6521	6739	6814	−32.98	−33.06	−33.09
	1000							5009	5222	4882	−32.30	−32.41	−32.23
Ca–Cin6	100	0.9994	0.9998	0.9993	1.16	1.16	1.11	42 714	45 066	55 832	−37.82	−37.96	−38.51
	300							15 456	16 171	18 903	−35.20	−35.32	−35.72
	500							9648	10 084	11 717	−33.99	−34.10	−34.49
	700							7054	7527	10 348	−33.18	−33.35	−34.17
	1000							5825	5765	8165	−32.69	−32.66	−33.56

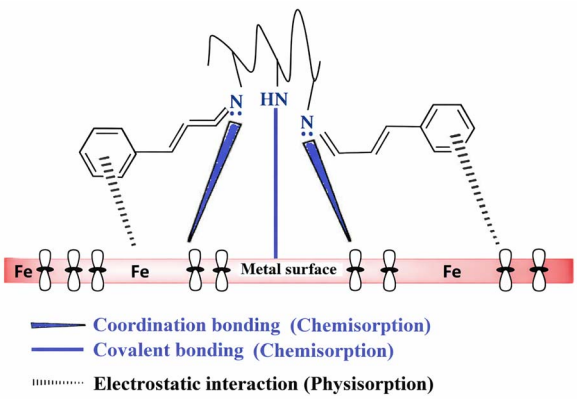

Fig. 12 Schematic of the chemisorption and physisorption probabilities of the Schiff base molecules on the 316L stainless steel surface, along with the proposed bonding.

4. Conclusions

In this study, the as-synthesized casein–cinnamaldehyde (cinnamyl casein) Schiff bases are used to create self-assembled monolayers (SAMs) on the surface of a medical-grade 316L stainless steel (316L SS). The proposed SAMs are electrochemically examined as anticorrosive compounds in a freshly prepared simulated body fluid (SBF) solution. As expected, there is a marked change in the corrosion behavior of stainless steel. The results can be summarized in some points. The SAMs of the Schiff base derivatives are formed on the SS surface. The Tafel polarization curves indicate that these polymeric compounds are classified as mixed-type inhibitors, predominantly anodic. The corrosion inhibition efficiency increases with the increase in the concentration of Schiff bases and the immersion times in their solutions. The maximum efficiency was found to exceed 90% at 1000 ppm after 120 minutes of immersion. These results show the superior performance of the treated 316L SS. Meanwhile, the untreated 316L SS steel alloy is already being used as an implant biomaterial. The corrosion inhibition efficiency of the studied Schiff bases is in the order of Ca–Cin1 < Ca–Cin2 < Ca–Cin3 < Ca–Cin4 < Ca–Cin5 < Ca–Cin6. The EIS results illustrate a charge transfer reaction, a one-time constant, and an increase in the phase angle. Additionally, the inhibition performance was optimized at 1000 ppm after 120 minutes of immersion, presenting good agreement with experimental measurements. Thermodynamic calculations indicate a comprehensive adsorption, involving both physical and chemical spontaneous adsorption that obeys the Langmuir adsorption isotherm. Future work will focus on

enhancing the adhesion of stainless steel surfaces to improve inhibition performance and durability for biomedical applications.

Author contributions

Conceptualization, T. M. T. and N. H.; data curation, A. H., A. N., S. M. A., T. M. T., and N. H.; investigation, A. H., N. H., T. M. T., and N. H.; formal analysis, A. H., A. N., S. M. A., J. E.-N., T. M. T., and N. H.; writing—original draft, A. H., A. N., S. M. A., J. E.-N., A. S. I. A., R. M. A. S., T. M. T. and N. H.; writing—review and editing, A. N., and T. M. T., and N. H. All authors have read and agreed to the published version of the manuscript.

Conflicts of interest

The authors declare no conflicts of interest.

Data availability

All experiments were carried out by the authors and no external data were used.

Fig. 1 was reproduced from our previous article: DOI: https://doi.org/10.1039/d5ra00852b.

The supporting data of this article have been included as part of the supplementary information (SI). Supplementary information is available. See DOI: https://doi.org/10.1039/d5ra06705g.

References

1 A. M. Abraham and S. Venkatesan, A review on application of biomaterials for medical and dental implants, *Proc. Inst. Mech. Eng., Part L*, 2023, **237**(2), 249–273, DOI: 10.1177/14644207221121981.
2 R. Agrawal, S. Singh, K. K. Saxena and D. Buddhi, A role of biomaterials in tissue engineering and drug encapsulation, *Proc. Inst. Mech. Eng., Part E*, 2025, **239**(4), 1626–1636, DOI: 10.1177//09544089221150740.
3 S. Todros, M. Todesco and A. Bagno, Biomaterials and their biomedical applications: from replacement to regeneration, *Processes*, 2021, **9**(11), 1949, DOI: 10.3390/pr9111949.
4 E. Davoodi, H. Montazerian, A. S. Mirhakimi, M. Zhianmanesh, O. Ibhadode, S. I. Shahabad, R. Esmaeilizadeh, E. Sarikhani, S. Toorandaz, S. A. Sarabi and R. Nasiri, Additively manufactured metallic biomaterials, *Bioact. Mater.*, 2022, **15**, 214–249, DOI: 10.1016/j.bioactmat.2021.12.027.
5 N. Eliaz, Corrosion of metallic biomaterials: A review, *Materials*, 2019, **12**(3), 407, DOI: 10.3390/ma12030407.
6 K. Vinchurkar, S. P. N. Bukke, P. Jain, J. Bhadoria, M. Likhariya, S. Mane, M. Suryawanshi, K. V. Veerabhadrappa, Z. Eftekhari and H. Onohuean, Advances in sustainable biomaterials: characterizations, and applications in medicine, *Discover Polym.*, 2025, **2**(1), 2, DOI: 10.1007/s44347-025-00014-8.
7 D. Shekhawat, A. Singh, A. Bhardwaj and A. Patnaik, A short review on polymer, metal and ceramic based implant materials, *IOP Conf. Ser.: Mater. Sci. Eng.*, 2021, **1017**(1), 012038, DOI: 10.1088/1757-899X/1017/1/012038.
8 S. Bose, S. F. Robertson and A. Bandyopadhyay, Surface modification of biomaterials and biomedical devices using additive manufacturing, *Acta Biomater.*, 2018, **66**, 6–22, DOI: 10.1016/j.actbio.2017.11.003.
9 N. Shayesteh Moghaddam, M. Taheri Andani, A. Amerinatanzi, C. Haberland, S. Huff, M. Miller, M. Elahinia and D. Dean, Metals for bone implants: Safety, design, and efficacy, *Biomanuf. Rev.*, 2016, **1**(1), 1, DOI: 10.1007/s40898-016-0001-2.
10 X. Hu, T. Wang, F. Li and X. Mao, Surface modifications of biomaterials in different applied fields, *RSC Adv.*, 2023, **13**(30), 20495–20511, DOI: 10.1039/d3ra02248j.
11 M. Kheirkhah, M. Fathi, H. R. Salimijazi and M. Razavi, Surface modification of stainless steel implants using nanostructured forsterite (Mg_2SiO_4) coating for biomaterial applications, *Surf. Coat. Technol.*, 2015, **276**, 580–586, DOI: 10.1016/j.surfcoat.2015.06.012.
12 N. Sultana, Y. Nishina and M. Z. I. Nizami, Surface modifications of medical grade stainless steel, *Coatings*, 2024, **14**(3), 248, DOI: 10.3390/coatings14030248.
13 R. Bhure, T. M. Abdel-Fattah, C. Bonner, F. Hall and A. Mahapatro, Stability of phosphonic self assembled monolayers (SAMs) on cobalt chromium (Co–Cr) alloy under oxidative conditions, *Appl. Surf. Sci.*, 2011, **257**(13), 5605–5612, DOI: 10.1016/j.apsusc.2011.01.055.
14 A. Mahapatro, D. M. Johnson, D. N. Patel, M. D. Feldman, A. A. Ayon and C. M. Agrawal, The use of alkanethiol self-assembled monolayers on 316L stainless steel for coronary artery stent nanomedicine applications: an oxidative and in vitro stability study, *Nanomed. Nanotechnol. Biol. Med.*, 2006, **2**(3), 182–190, DOI: 10.1016/j.nano.2006.07.006.
15 A. Mahapatro, T. D. Matos Negron and A. S. Gomes, Nanostructured self assembled monolayers on magnesium for improved biological performance, *Mater. Tech.*, 2016, **31**(13), 818–827, DOI: 10.1080/10667857.2016.1222053.
16 N. Hassan, D. R. Ramadan, A. A. Elbardan, A. Ebrahim and S. N. Khattab, Electrochemical evaluation of synthesized *s*-triazine derivatives for improving 316L stainless steel for biomedical applications, *Monatsh. Chem.*, 2019, **150**(10), 1761–1771, DOI: 10.1007/s00706-019-02499-z.
17 N. Hassan, A. Hendy, A. Ebrahim and T. M. Tamer, Synthesis and evaluation of novel O-functionalized aminated chitosan derivatives as antibacterial, antioxidant and anticorrosion for 316L stainless steel in simulated body fluid, *J. Saudi Chem. Soc.*, 2021, **25**(12), 101368, DOI: 10.1016/j.jscs.2021.101368.
18 G. A. Buckholtz and E. S. Gawalt, Effect of alkyl chain length on carboxylic acid SAMs on Ti-6Al-4V, *Materials*, 2012, **5**(7), 1206–1218, DOI: 10.3390/ma5071206.
19 A. Mahapatro, Bio-functional nano-coatings on metallic biomaterials, *Mater. Sci. Eng., C*, 2015, **55**, 227–251, DOI: 10.1016/j.msec.2015.05.018.

20 N. Hassan and R. Holze, Surface enhanced Raman spectroscopy of self-assembled monolayers of 2-mercaptopyridine on a gold electrode, *Russ. J. Electrochem.*, 2012, **48**(4), 401–411, DOI: 10.1134/S1023193512030056.
21 L. Feng, S. Zheng, H. Zhu, X. Ma and Z. Hu, Detection of corrosion inhibition by dithiane self-assembled monolayers (SAMs) on copper, *J. Taiwan Inst. Chem. Eng.*, 2023, **142**, 104610, DOI: 10.1016/j.jtice.2022.104610.
22 S. Chen, H. Zhang, Y. Qiang, B. Tan, Y. Wu and S. Chen, Self-assembled monolayers of Ginkgo biloba exocarp extract for corrosion protection of copper, *J. Mol. Liq.*, 2023, **382**, 121941, DOI: 10.1016/j.molliq.2023.121941.
23 D. S. Chauhan, A. A. Sorour, V. S. Saji and M. A. Quraishi, Green corrosion inhibitors based on biomacromolecules and macrocycles: A review, *Sustainable Chem. Pharm.*, 2023, **36**, 101295, DOI: 10.1016/j.scp.2023.101295.
24 A. Pandey, B. Singh, C. Verma and E. E. Ebenso, Synthesis, characterization and corrosion inhibition potential of two novel Schiff bases on mild steel in acidic medium, *RSC Adv.*, 2017, **7**(74), 47148–47163, DOI: 10.1039/C7RA08887F.
25 K. R. Ansari, D. S. Chauhan, M. A. Quraishi, M. A. Mazumder and A. Singh, Chitosan Schiff base: an environmentally benign biological macromolecule as a new corrosion inhibitor for oil & gas industries, *Int. J. Biol. Macromol.*, 2020, **144**, 305–315, DOI: 10.1016/j.ijbiomac.2019.12.106.
26 L. Ma, W. Li, S. Zhu, L. Wang and S. Guan, Corrosion inhibition of Schiff bases for Mg-Zn-Y-Nd alloy in normal saline: Experimental and theoretical investigations, *Corros. Sci.*, 2021, **184**, 109268, DOI: 10.1016/j.corsci.2021.109268.
27 X. Lai, J. Hu, T. Ruan, J. Zhou and J. Qu, Chitosan derivative corrosion inhibitor for aluminum alloy in sodium chloride solution: A green organic/inorganic hybrid, *Carbohydr. Polym.*, 2021, **265**, 118074, DOI: 10.1016/j.carbpol.2021.11807.
28 Z. Zhang, Q. Song, Y. Jin, Y. Feng, J. Li and K. Zhang, Advances in Schiff base and its coating on metal biomaterials—A review, *Metals*, 2023, **13**(2), 386, DOI: 10.3390/met13020386.
29 A. A. Altalhi, Novel N-heterocyclic Schiff base based on Isatin derivative as a sustainable, eco-friendly, and highly efficiency corrosion inhibitor for carbon steel in sulfuric acid medium: Electrochemical and Computational investigation, *Int. J. Electrochem. Sci.*, 2024, **19**(1), 100449, DOI: 10.1016/j.ijoes.2023.100449.
30 A. Hendy, N. Hassan, J. El-Nady, A. S. Ahmed, R. M. AbouShahba and T. M. Tamer, Enhancement of biological properties in casein protein through functionalization with cinnamaldehyde via Schiff base bonding: antibacterial and antioxidant effects, *RSC Adv.*, 2025, **15**(33), 27300, DOI: 10.1039/d5ra00852b.
31 N. Hassan and N. A. Abdel Ghany, Corrosion of biomaterials: anodic treatment and evaluation of 316L stainless steel in simulated body fluid. Corrosion Engineering, *Sci. Technol.*, 2017, **52**(4), 267–275, DOI: 10.1080/1478422X.2016.1267932.
32 T. Kokubo and H. Takadama, How useful is SBF in predicting in vivo bone bioactivity?, *Biomaterials*, 2006, **27**(15), 2907–2915, DOI: 10.1016/j.biomaterials.2006.01.017.
33 Ch. Wenck, N. Meier, E. Heinrich, V. Grützner, F. Wiekhorst and R. Bleul, Design and characterisation of casein coated and drug loaded magnetic nanoparticles for theranostic applications, *RSC Adv.*, 2024, **14**, 26388, DOI: 10.1039/d4ra02626h.
34 Y. Qiang, S. Zhang and L. Wang, Understanding the adsorption and anticorrosive mechanism of DNA inhibitor for copper in sulfuric acid, *Appl. Surf. Sci.*, 2019, **492**, 228–238, DOI: 10.1016/j.apsusc.2019.06.190.
35 M. H. Sliem, M. Afifi, A. Bahgat Radwan, E. M. Fayyad, M. F. Shibl, F. E. T. Heakal and A. M. Abdullah, AEO7 surfactant as an eco-friendly corrosion inhibitor for carbon steel in HCl solution, *Sci. Rep.*, 2019, **9**(1), 2319, DOI: 10.1038/s41598-018-37254-7.
36 N. J. Maduelosi and N. B. Iroha, Insight into the adsorption and inhibitive effect of spironolactone drug on C38 carbon steel corrosion in hydrochloric acid environment, *J. Bio-Tribo-Corros.*, 2021, **7**(1), 6, DOI: 10.1007/s40735-020-00441-z.
37 A. El Aatiaoui, M. Koudad, T. Chelfi, S. Erkan, M. Azzouzi, A. Aouniti, K. Savaş, M. Kaddouri, N. Benchat and A. Oussaid, Experimental and theoretical study of new Schiff bases based on imidazo (1, 2-a) pyridine as corrosion inhibitor of mild steel in 1M HCl, *J. Mol. Struct.*, 2021, **1226**, 129372, DOI: 10.1016/j.molstruc.2020.129372.
38 N. M. Ahmed, S. M. Ali, M. F. El-Saka, A. A. Elhenawy and N. Hassan, Eco-Friendly and Sustainable Corrosion Inhibition: Practical and Theoretical Investigations of Applying Self-Assembled Monolayers Approach Based on Gelatin (gelatin-SAMs) upon the Carbon Steel Surface in an Acidic medium, *Mater. Today Commun.*, 2025, **48**, 113389, DOI: 10.1016/j.mtcomm.2025.113389.
39 R. Karthik, P. Muthukrishnan, A. Elangovan, M. M. Srividhya, B. Jeyaprabha and P. Prakash, Adsorption and corrosion inhibiting behavior of a new S-triazine derivative, *Prot. Met. Phys. Chem.*, 2015, **51**(4), 667–679, DOI: 10.1134/S2070205115040152.
40 E. B. Ituen, O. Akaranta and S. A. Umoren, N-acetyl cysteine based corrosion inhibitor formulations for steel protection in 15% HCl solution, *J. Mol. Liq.*, 2017, **246**, 112–118, DOI: 10.1016/j.molliq.2017.09.040.
41 Y. Zhou, S. Xu, L. Guo, S. Zhang, H. Lu, Y. Gong and F. Gao, Evaluating two new Schiff bases synthesized on the inhibition of corrosion of copper in NaCl solutions, *RSC Adv.*, 2015, **5**(19), 14804–14813, DOI: 10.1039/C4RA14449J.
42 A. A. Ali and W. I. El-Dougdoug, Preparation and evaluation of amido poly amine surfactant based on Melia azedarach seeds oil as corrosion inhibitor of C-steel in 2.0 M HCl pickling medium, *Green Chem. Lett. Rev.*, 2017, **10**(4), 346–358, DOI: 10.1080/17518253.2017.1385857.
43 H. Lgaz, K. S. Bhat, R. Salghi, S. Jodeh, M. Algarra, B. Hammouti, I. H. Ali and A. Essamri, Insights into corrosion inhibition behavior of three chalcone derivatives for mild steel in hydrochloric acid solution, *J. Mol. Liq.*, 2017, **238**, 71–83, DOI: 10.1016/j.molliq.2017.04.124.
44 K. Haruna, I. B. Obot, N. K. Ankah, A. A. Sorour and T. A. Saleh, Gelatin: A green corrosion inhibitor for carbon

steel in oil well acidizing environment, *J. Mol. Liq.*, 2018, **264**, 515–525, DOI: 10.1016/j.molliq.2018.05.058.

45 C. Liang, P. Wang, B. Wu and N. Huang, Inhibition of copper corrosion by self-assembled monolayers of triazole derivative in chloride-containing solution, *J. Solid State Electrochem.*, 2010, **14**(8), 1391–1399, DOI: 10.1007/s10008-009-0956-5.

46 Y. Qiang, S. Fu, S. Zhang, S. Chen and X. Zou, Designing and fabricating of single and double alkyl-chain indazole derivatives self-assembled monolayer for corrosion inhibition of copper, *Corros. Sci.*, 2018, **140**, 111–121, DOI: 10.1016/j.corsci.2018.06.012.

47 C. Verma, L. O. Olasunkanmi, E. E. Ebenso and M. A. Quraishi, Substituents effect on corrosion inhibition performance of organic compounds in aggressive ionic solutions: a review, *J. Mol. Liq.*, 2018, **251**, 100–118, DOI: 10.1016/j.molliq.2017.12.055.

48 U. J. Naik and N. K. Shah, Electrochemical and Adsorption Behaviour Study for Corrosion Inhibition Efficiency and Position of Group in Schiff Base for Aluminium in Acidic Media, *Int. J. Innov. Res. Sci. Eng. Technol.*, 2014, **3**(3), 10422–10431.

49 N. Rhazzane, A. Jmiai, R. El Brychy and H. Zejli, Corrosion inhibition potential of a green inhibitor "Red Algae" for copper in 1 M sulfuric acid solution determined by electrochemical measurement, weight loss technique, UV–visible, FTIR spectroscopy and complemented with surface analysis (SEM–EDS), *J. Bio- Tribo-Corros.*, 2023, **9**(2), 31, DOI: 10.1007/s40735-023-00747-8.

50 M. M. Khowdiary, N. A. Taha, A. A. Barqawi, A. A. Elhenawy, M. Sheta and N. Hassan, Theoretical and experimental evaluation of the anticorrosion properties of new Coumarin's derivatives, *Alexandria Eng. J*, 2022, **61**, 6937–6948, DOI: 10.1016/j.aej.2021.12.037.

51 M. Rbaa, M. Galai, F. Benhiba, I. B. Obot, H. Oudda, M. Ebn Touhami, B. Lakhrissi and A. Zarrouk, Synthesis and investigation of quinazoline derivatives based on 8-hydroxyquinoline as corrosion inhibitors for mild steel in acidic environment: experimental and theoretical studies, *Ionics*, 2019, **25**(7), 3473–3491, DOI: 10.1007/s11581-018-2817-7.

52 S. K. Gupta, R. K. Mitra, M. Yadav, O. Dagdag, A. Berisha, B. B. Mamba, T. T. I. Nkambule, E. E. Ebenso and S. K. Singh, Electrochemical, surface morphological and computational evaluation on carbohydrazide Schiff bases as corrosion inhibitor for mild steel in acidic medium, *Sci. Rep.*, 2023, **13**, 15108, DOI: 10.1038/s41598-023-41975-9.

53 M. Ashour, S. M. Ali, H. F. Khalil, M. F. Bakr, A. A. Elhenawy, M. A. Abu-Saied and N. Hassan, Influence of a polymeric azetidinium salt cationic polymer as an anticorrosion agent in an acidic medium for carbon steel alloy: Practical and theoretical aspects, *Mater. Chem. Phys.*, 2026, **348**, 131714, DOI: 10.1016/j.matchemphys.2025.131714.

54 A. Hendy, J. El-Nady, N. Hassan, T. M. Tamer, A. S. I. Ahmed and R. M. Abou Shahba, Corrosion inhibition of casein as a natural protein for 316L stainless steel in simulated body fluid, *Al-Azhar Bull. Sci.*, 2020, **31**(1), 11–18.

55 N. Hassan, A. M. Ramadan, S. Khalil, N. A. A. Ghany, A. M. Asiri and R. M. El-Shishtawy, Experimental and computational investigations of a novel quinoline derivative as a corrosion inhibitor for mild steel in salty water, *Colloids Surf., A*, 2020, **607**, 125454, DOI: 10.1016/j.colsurfa.2020.125454.

56 M. Rbaa, M. Galai, A. S. Abousalem, B. Lakhrissi, M. E. Touhami, I. Warad and A. Zarrouk, Synthetic, spectroscopic characterization, empirical and theoretical investigations on the corrosion inhibition characteristics of mild steel in molar hydrochloric acid by three novel 8-hydroxyquinoline derivatives, *Ionics*, 2020, **26**(1), 503–522, DOI: 10.1007/s11581-019-03160-9.

57 M. El Faydy, F. Benhiba, H. About, Y. Kerroum, A. Guenbour, B. Lakhrissi, I. Warad, C. Verma, E. S. M. Sherif, E. E. Ebenso and A. Zarrouk, Experimental and computational investigations on the anti-corrosive and adsorption behavior of 7-N, N'-dialkyaminomethyl-8-Hydroxyquinolines on C40E steel surface in acidic medium, *J. Colloid Interface Sci.*, 2020, **576**, 330–344, DOI: 10.1016/j.jcis.2020.05.010.

58 Y. Qiang, H. Li and X. Lan, Self-assembling anchored film basing on two tetrazole derivatives for application to protect copper in sulfuric acid environment, *J. Mater. Sci. Technol.*, 2020, **52**, 63–71, DOI: 10.1016/j.jmst.2020.04.005.

59 P. Singh, V. Srivastava and M. A. Quraishi, Novel quinoline derivatives as green corrosion inhibitors for mild steel in acidic medium: electrochemical, SEM, AFM, and XPS studies, *J. Mol. Liq.*, 2016, **216**, 164–173, DOI: 10.1016/j.molliq.2015.12.086.

60 A. I. Ali and Y. S. Mahrous, Corrosion inhibition of C-steel in acidic media from fruiting bodies of Melia azedarach L extract and a synergistic Ni^{2+} additive, *RSC Adv.*, 2017, **7**(38), 23687–23698, DOI: 10.1039/c7ra00111h.

61 B. Tan, S. Zhang, W. Li, X. Zuo, Y. Qiang, L. Xu, J. Hao and S. Chen, Experimental and theoretical studies on inhibition performance of Cu corrosion in 0.5 M H_2SO_4 by three disulfide derivatives, *J. Ind. Eng. Chem.*, 2019, **77**, 449–460, DOI: 10.1016/j.jiec.2019.05.011.

62 S. K. Saha, A. Dutta, P. Ghosh, D. Sukul and P. Banerjee, Adsorption and corrosion inhibition effect of Schiff base molecules on the mild steel surface in 1 M HCl medium: a combined experimental and theoretical approach, *Phys. Chem. Chem. Phys.*, 2015, **17**(8), 5679–5690, DOI: 10.1039/c4cp05614k.

63 D. S. Chauhan, C. Verma and M. A. Quraishi, Molecular structural aspects of organic corrosion inhibitors: Experimental and computational insights, *J. Mol. Struct.*, 2021, **1227**, 129374, DOI: 10.1016/j.molstruc.2020.129374.

64 N. Hassan and R. Holze, A comparative electrochemical study of electrosorbed 2-and 4-mercaptopyridines and their application as corrosion inhibitors at C60 steel, *J. Chem. Sci.*, 2009, **121**(5), 693–701, DOI: 10.1007/s12039-009-0083-y.

65 H. M. A. El-Lateef, T. El-Dabea, M. M. Khalaf and A. M. Abu-Dief, Innovation of imine metal chelates as corrosion inhibitors at different media: A collective study, *Int. J. Mol. Sci.*, 2022, **23**(16), 9360, DOI: 10.3390/ijms23169360.

66 L. H. Madkour and S. K. Elroby, Inhibitive properties, thermodynamic, kinetics and quantum chemical calculations of polydentate Schiff base compounds as corrosion inhibitors for iron in acidic and alkaline media, *Int. J. Ind. Chem.*, 2015, **6**(3), 165–184, DOI: 10.1007/s40090-015-0039-7.

67 A. A. Al-Amiery, A. A. H. Kadhum, A. Kadihum, A. B. Mohamad, C. K. How and S. Junaedi, Inhibition of mild steel corrosion in sulfuric acid solution by new Schiff base, *Materials*, 2014, **7**(2), 787–804, DOI: 10.3390/ma7020787.

68 N. Rezki, J. Haque, A. Aljuhani, W. M. N. W. Nik, W. M. K. W. M. Ikhmal, M. A. Quraishi and M. R. Aouad, Aluminium alloy corrosion prevention in 1M HCl via novel 1, 2, 3-triazole-aromatic acetamide molecular conjugates: Effect of the substituent and DFT study, *J. Mol. Struct.*, 2025, **1338**, 142168, DOI: 10.1016/j.molstruc.2025.142168.

69 A. El Amri, N. El-Aouni, O. Dagdag, A. El Amri, I. Rachid, A. Berisha, H. Kim, R. Haldhar, M. Rafik, W. W. Nik and M. E. Touhami, Assessment of a New Epoxy Resin for Corrosion Prevention of Mild Steel in HCl Environment: Experimental and Theoretical Analyses, *Electrocatalysis*, 2025, **16**, 526–547, DOI: 10.1007/s12678-025-00933-x.